Original Research

In vitro and *in vivo* characterization of the anticancer activity of Thai stingless bee (*Tetragonula laeviceps*) cerumen

Pongvit Nugitrangson[1], Songchan Puthong[2], Tawin Iempridee[3], Wittaya Pimtong[3], Surachai Pornpakakul[4] and Chanpen Chanchao[5]

[1]Program in Biotechnology, Faculty of Science, Chulalongkorn University, Bangkok 10330, Thailand; [2]Institute of Biotechnology and Genetic Engineering, Chulalongkorn University, Bangkok 10330, Thailand; [3]National Nanotechnology Center, National Science and Technology Development Agency, Thanon Phahonyothin, Tambon Khlong Nueng, Amphoe Khlong Luang, Pathum Thani 12120, Thailand; [4]Research Centre for Bioorganic Chemistry, Department of Chemistry, Faculty of Science, Chulalongkorn University, Bangkok 10330, Thailand; [5]Department of Biology, Faculty of Science, Chulalongkorn University, Bangkok 10330, Thailand
Corresponding authors: Surachai Pornpakakul. Email: surachai.p@chula.ac.th; Chanpen Chanchao. Email: chanpen@sc.chula.ac.th

Abstract

Tetragonula laeviceps cerumen was sequentially extracted with 80% (v/v) methanol, dichloromethane, and hexane and also in the reverse order. By the MTT assay and the respective 50% inhibition concentration value, the most active fraction was further purified to apparent homogeneity by bioassay-guided silica gel column chromatography. α-Mangostin was identified by high-resolution electrospray ionization mass spectrometry and nuclear magnetic resonance analyses. It had a potent cytotoxicity against the BT474, Chago, Hep-G_2, KATO-III, and SW620 cell lines (IC_{50} values of 1.22 ± 0.03, 2.25 ± 0.20, 0.94 ± 0.01, 0.88 ± 0.16, and 1.50 ± 0.39 μmol/L, respectively). The *in vitro* cytotoxicity of α-mangostin against the five human cancer cell lines and primary fibroblasts was further characterized by real-time impedance-based analysis. Interestingly, α-mangostin was more cytotoxic against the cancer-derived cell lines than against the primary fibroblasts. Later, the migration assay was performed by continuously measuring the attachment of cells to the plate electrodes at the bottom of the transwell membrane. The combined caspase-3 and -7 activities were assayed by the Caspase-Glo® 3/7 kit. It showed that the cytotoxic mechanism involved caspase-independent apoptosis, while at low (non-toxic) concentrations α-mangostin did not significantly alter cell migration. Furthermore, the *in vivo* cytotoxicity and angiogenesis were determined by alkaline phosphatase staining in zebrafish embryos along with monitoring changes in the transcript expression level of two genes involved in angiogenesis (*vegfaa* and *vegfr2*) by quantitative real-time reverse transcriptase- polymerase chain reaction. It was found that the *in vivo* cytotoxicity of α-mangostin against zebrafish embryos had a 50% lethal concentration of 9.4 μM, but no anti-angiogenic properties were observed in zebrafish embryos at 9 and 12 μM even though it downregulated the expression of *vegfaa* and *vegfr2* transcripts. Thus, α-mangostin is a major active compound with a potential anticancer activity in *T. laeviceps* cerumen in Thailand.

Keywords: α-mangostin, cancer, cerumen, cytotoxicity, Tetragonula laeviceps

***Experimental Biology and Medicine* 2016; 241: 166–176. DOI: 10.1177/1535370215600102**

Introduction

Stingless bees are social insects in the family Apidae.[1] In Thailand, *Tetragonula laeviceps* is one of the native stingless bees and is widely dispersed, especially in Chantaburi, Chiang Mai, and Nan provinces where it is subject to meliniponiculture (stingless bee culturing).[2] The inside of its hive has many cells (called pots) that are used to store larvae, pollen, honey, and other products.[3] The main material used in the construction of these pots is cerumen, a dark brown and sticky material that is a mixture of pure wax and propolis.[4] Cerumen is not only the main component of storage pots and brood cells, but it is also the material used for involucrum, a cerumen sheet that covers the brood section to control the temperature and protect the brood cells.

The products of honey bees, including stingless bees, such as honey, propolis, wax, pollen, and venom, have been reported to have many bioactivities and pharmaceutical benefits, including anti-viral,[5] antimicrobial,[6] anti-oxidant,[7] anti-inflammatory,[8] anti-cholesterol,[9] and antiproliferative activities.[10] In addition, interest in the potential bioactivity of mixed bee products, such as geopropolis and cerumen, has increased. Geopropolis, which is a

mixture of plant resins, waxes and earth collected by stingless bees (Meliponinae), was reported to have a high antioxidant activity.[11] Thus, cerumen, which is also a mixed product, could have interesting bioactivities. The limited research to date on the composition of cerumen has reported that pimaric acid, iso-pimaric acid, and gallic acid from the crude ethanol extract of *T. carbonaria* cerumen in Australia could inhibit 5-lipoxygenase, an inflammatory modulator.[12]

The chemical and biological properties of bee products are known to depend on the bee species, nearby plants, climate, and region, while their detection depends on the separation technique utilized.[13] In this research, the cerumen of *T. laeviceps* collected from Chantaburi province (Thailand) was investigated in terms of the *in vitro* antiproliferative/cytotoxic activity (hereafter ''cytotoxicity'') against five human cancer-derived cell lines. Cancer is a group of severe diseases that all share a common phenotype of an abnormal cell cycle and aberrant apoptosis responses.[14] They are fatal without treatment and cause a high rate of death globally. As for treatment, most cancers once diagnosed cannot be simply surgically removed and so require destructive radiotherapy or chemotherapy, the latter of which especially can have many adverse severe side effects to patients. Moreover, some cancer cells have evolved resistance to current chemotherapeutic agents. For example, some breast cancers have significant resistance to doxorubicin (doxil) and Docataxel, resulting in a very high 50% inhibition concentration (IC_{50}) to these two drugs of 403.6 and 68.3 μg/mL, respectively.[15] Hence, it is still important to find novel agents with a high efficacy for the treatment of different cancers, especially from natural products. This is because some 47.1% of approved anticancer drugs were reported to be either unmodified natural compounds or semisynthetic derivatives or synthesized molecules based on the chemical structure of natural compounds.[16]

This research aimed to separate and analyze the cytotoxic components in the cerumen obtained from *T. laeviceps* from one locality within Thailand by sequential partition extraction with three different organic solvents. All crude extracts were then tested for their *in vitro* cytotoxicity against five human cancer-derived cell lines using the 3-(4,5-dimethyl-thiazol-2-yl)2,5-diphenyl-tetrazolium bromide (MTT) assay. The most active crude extract of cerumen was then further fractionated by silica gel column chromatography (CC) following the MTT-based cytotoxic activity to apparent homogeneity, as observed by one dimensional thin layer chromatography (1D-TLC) and characterized by ^{1}H- and ^{13}C-nuclear magnetic resonance (NMR) and high-resolution electrospray ionization mass spectroscopy (HRESIMS).

Following identification of the bioactive compound, real-time impedance-based cell viability analysis was used to compare the cytotoxicity in human primary fibroblast and cancer-derived cell lines. In addition, the effects of the pure compound on the cell morphology, cell migration, and activation of caspase 3/7 were investigated. Finally, the *in vivo* cytotoxicity of the pure compound and its effects on angiogenesis were examined in zebrafish embryos.

Material and methods

Sample collection

Cerumen from *T. laeviceps* was collected from hives in a mangosteen (*Garcinia mangostana*) and rambutan (*Nephelium lappaceum*) orchard and meliniponiculture complex in Makham district, Chantaburi province, Thailand in May, 2012. It was wrapped in an aluminum foil and kept in the dark at −20°C until used.

Extraction procedure

Cerumen (200 g) was cut into small pieces and suspended in 900 mL of 80% (v/v) methanol (MeOH) and shaken at 15°C, 100 r/min for 18 h. The suspension was then clarified by centrifugation (5862 × *g*, 20°C for 15 min) and the supernatant harvested and evaporated to give the crude methanol extract (CME) (9.7 g). The residual cerumen pellet was then extracted as above except with 900 mL of dichloromethane (DCM) (104 g) with the evaporated supernatant yielding the crude DCM extract (CDE). Finally, the partitioning of the residual cerumen pellet with 900 mL of hexane as above yielded the crude hexane extract (CHE) (47 g). In addition, a different portion of fresh cerumen (70 g) was sequentially extracted as above except in the reverse solvent order of hexane, DCM and 80% (v/v) MeOH to yield the reCHE (5.8 g), reCDE (19 g), and reCME (27 g), respectively. These six crude extracts were kept in the dark at −20°C until tested for their *in vitro* antiproliferative/cytotoxic activity by the MTT assay.

The crude extract that exhibited the highest cytotoxicity (reDCE) was subjected to silica gel CC (silica gel 60, Merck [ø 5 cm × 50 cm]) eluting with hexane, ethyl acetate, and MeOH in a stepwise fashion. Fractions with a similar TLC profile after ceric ammonium molybdate staining were combined and each combined fraction was then tested for its cytotoxicity on the same cell lines as above using the MTT assay. Those fractions exhibiting a high activity (in terms of a low IC_{50} value) against all five human cancer cell lines were further fractionated by silica gel CC (silica gel 60, Merck [ø 3 cm × 60 cm]) eluting with DCM-MeOH in a stepwise fashion and collecting 5 mL subfractions. As before, subfractions with a similar TLC profile were combined. The obtained fractions with significant cytotoxicity (low IC_{50} value) were then subject to silica gel CC (ø 2.5 cm × 50 cm) and eluted with DCM-MeOH in a stepwise fashion, as required to obtain apparent homogeneity, as indicated in the results. The compounds were then characterized by NMR and HRESIMS for identification.

Characterization procedures

The ^{1}H- and ^{13}C-NMR spectra were recorded at 400 and 100 MHz, respectively, on Varian Model Mercury (400 MHz) and Bruker Model AVANCE (400 MHz) instruments, respectively. Deuterated chloroform ($CDCl_3$) was used as the solvent and the chemical shifts were referenced to the signals of the residual solvent at δ_H 7.26 ppm and δ_C 77.16 ppm. The HRESIMS was recorded on Bruker

Model micrOTOF spectrometer (Micromass UK Ltd.). The apparent purity of fractions and their composition was monitored by TLC using 0.2 mm silicagel 60 F_{254} on an aluminium sheet (Merck) as the stationary phase and detection by UV light and ceric ammonium molybdate staining. For the chromatographic separations, silica gel 60 (230–400 mesh ASTM, Merck) and silica gel 60 RP-18 (40–60 μm) (Merck) were used as the stationary phase for normal CC and for reverse phase CC, respectively, and eluted with the indicated mobile phases.

Human cancer-derived cell lines

For assaying the *in vitro* cytotoxicity during cerumen extraction, five human cancer-derived cell lines were used in this study that were originally derived from ductol carcinoma or breast cancer (BT 474, ATCC® HTB20™), undifferentiated lung or lung cancer (Chago, National Cancer Institute, Thailand), hepatoblastoma or liver cancer (Hep-G_2, ATCC® HB8065™), gastric carcinoma or stomach cancer (KATO-III, ATCC® HTB103™), and colon adenocarcinoma (SW620, ATCC® CCL227™). In addition, the non-transformed human male skin fibroblast cell line (CCD-986sk, ATCC® CRL-1947™) was used for comparison. These cell lines were cultured in complete medium (CM) comprising RPMI 1640 medium with 5% (v/v) fetal bovine serum (FBS) for the cancer cell lines (CM_R) and Basal Isscove medium with 5% (v/v) FBS for CCD-986sk (CM_B). For seeding the cells, 1×10^5 cells were transferred to 5 mL of the respective CM in a 25-cm^2 flask and were incubated at 37°C with 5% (v/v) CO_2. They were re-passaged when at 70–80% confluency.

For the cytotoxicity assay for real-time impedance-based analysis, HeLa (ATCC® CCL2™) and the primary human fibroblast (ATCC® CRL-2708™) cell lines were grown in CM_D (DMEM (Hyclone/Thermo Scientific) supplemented with 10% (v/v) FBS, 100 units/mL penicillin and 100 μg/mL streptomycin), otherwise as above.

Cytotoxicity evaluation by the MTT assay

For each cell line, 5×10^3 cells in 198 μL of the respective CM were transferred per well of a 96-well plate. After they had been incubated at 37°C with 5% (v/v) CO_2 overnight, 2 μL of the test sample at different concentrations in dimethylsufoxide (DMSO) or 2 μL of pure DMSO as the negative solvent control, was added and incubated at 37°C with 5% CO_2 (v/v) for another 72 h. In addition, doxil and 5-fluorouracil (5-FU) in 2 μL DMSO were used as a positive control. After 72 h of exposure, the cytotoxicity was assayed by MTT.

After 72 h of incubation with the test substance, 10 μL of MTT solution (5 mg/mL in sterile normal saline) was added into each well and incubated as before for 4 h. The supernatant was then aspirated out and a mixture of 150 μL of DMSO and 25 μL of 0.1 M glycine was added and gently mixed to dissolve the purple–blue formazan crystals prior to measuring the absorbance at 540 nm (A_{540}) by a microplate reader. The number of viable cells as a relative percentage of that of the DMSO only control (set to 100%) was calculated from equation (1)

$$\%\,\text{viable cells} = (A_{540}\ \text{of sample}/A_{540}\ \text{of control}) \times 100 \quad (1)$$

The IC_{50} value was determined from a plot of the percentage of viable cells against the concentration of the test extract or sample. In addition, the cell morphology was observed and photographed at 0, 24, 48, and 72 h incubation using an inverted light microscope connected to a camera.

Cytotoxicity assay by real-time impedance-based analysis

The CRL-2708™ (1500 cells/well), HeLa (3000 cells/well) and HT29 (5000 cells/well) cell lines were seeded into 100 μL of CM_D in a 96 ×E-Plate. The impedance value of each well was automatically measured every 30 min using an xCELLigence real-time cell analyzer dual-plate (RTCA DP) Instrument (ACEA Biosciences) and expressed as an arbitrary unit called the cell index. The cell index at each time point is defined as the cell-sensor impedance of the well containing cells after subtracting the background impedance of the well with the media alone. Cells were then treated with 50 μL of the indicated concentration of α-mangostin in DMSO or DMSO alone (solvent control) in CM_D when the cells reached the log growth phase (cell index∼1). The cell index was then monitored every 30 min for another 72 h, and the rate of cell proliferation was determined by calculating the slope of the line between two given time points.

Real-time cell migration assay

The rate of cell migration was monitored in real time with the xCELLigence RTCA DP device (ACEA Biosciences) as described in the supplier's instruction manual. Briefly, CM_D was added to each well of the lower chamber of a two-chamber device separated by a porous membrane (CIM-plate). A total of 30,000 HeLa cells in 100 μL of FBS-free CM_D media were seeded into each well of the upper chamber of the CIM-plate. Cells were settled for 30 min at room temperature before being placed back to the RTCA DP in an incubator at 37°C with 5% CO_2. When the cells migrate through the pores to the bottom side of the membrane (where the electrodes reside), the electrical impedance of the integrated gold microelectrodes increases. The electrical impedance is displayed as an arbitrary unit (cell index) and represents the capacity for cell migration, where the slope of the curve is related to the average velocity of cell migration. The cell index was measured every 15 min for approximately 16 h. Subsequently, cells were treated with 20 μL of the indicated final concentration of α-mangostin in DMSO, or DMSO only, in FBS-free CM_D. The cell index was then measured every 15 min for up to 56 h with the RTCA software.

Combined caspase 3/7 assay

HeLa (3500 cells/well) or CRL-2708™ (2000 cells/well) cell lines were seeded into a 96-well plate for 48 h in CM_D and

treated with the respective concentration of α-mangostin for another 48 h. The combined caspase 3/7 activity was analyzed in triplicates using the Caspase-Glo® 3/7 Assay (Promega) according to the manufacturer's protocol with some modifications. Briefly, after aspirating the medium, 30 μL of Caspase-Glo reagent and 20 μL of 1 ×PBS were added to each well and the samples were incubated at room temperature for 30 min. Subsequently, 90 μL of 1 ×PBS was added to each well and 100 μL of the reaction mixture was transferred to a white 96-well microplate. The caspase activities were measured using a SpectraMax® L Microplate Luminometer (Molecular Devices).

Zebrafish embryo toxicity and angiogenesis assays

Zebrafish embryos were maintained within the National Nanotechnology Center and were raised at 28.5°C under a 14 h light/10 h dark photoperiod. The α-mangostin toxicity against Zebrafish embryos was evaluated according to the OECD guideline 236. Fertilized eggs were collected under a stereomicroscope (Olympus SZX7, Tokyo, Japan) within 3 h post fertilization (hpf). The embryos were transferred at 10 embryos/well to a 24-well plate and α-mangostin in DMSO was diluted in the zebrafish embryo medium to a final concentration of 0 (DMSO solvent control), 3, 6, 9, 12, and 15 μM. In order to inhibit pigmentation, the embryo medium with 0.006% (w/v) of 1-phenyl 2-thiourea was used. At 72 hpf, the number of dead embryos was quantified and the α-mangostin toxicity, as the 50% lethal concentration (LC_{50}), was derived using SigmaPlot software. The surviving embryos were fixed in 4% (w/v) paraformaldehyde and used for a subintestinal vessel (SIV) assay, performed by alkaline phosphatase staining as described previously.[12] Briefly, fixed embryos were dehydrated in methanol and stored at −20°C overnight. After 30 min of permeabilization in cold acetone, embryos were washed with phosphate buffered saline tween-20 (PBST) and incubated in staining buffer (100 mM Tris-HCl [pH 9.5], 50 mM $MgCl_2$, 100 mM NaCl, and 0.1% Tween-20). The colorimetric detection of alkaline phosphatase activity was initiated by adding nitro blue tetrazolium/5-bromo-4-chloro-3-indolyl phosphate (NBT/BCIP, Roche). The stained embryos were examined under an Olympus SZX7 stereomicroscope.

Gene expression analysis by quantitative real-time reverse transcriptase PCR

The transcript levels of the vascular endothelial growth factor *vegfaa* and *vegfr2* genes in Zebrafish embryos treated with 0 (DMSO solvent control), 9 or 12 μM of α-mangostin were analyzed by two-stage quantitative real-time reverse transcriptase PCR (qrtRT-PCR). Embryos were homogenized in lysis buffer (buffer RLT) using a hand pistol and then total RNA was extracted using the RNeasy mini kit (QIAGEN) and treated with RNase-free DNaseI. In the first stage, the total RNA was converted to cDNA with the Maxima cDNA synthesis kit (Thermo Scientific) using oligo-dT and random primers. The synthesized cDNA was used as the template for the second-stage qrt-PCR, which was performed in a Biorad CFX96 Touch (Biorad) using a Luminaris Color HiGreen qPCR Master Mix (Thermo Scientific). The amplification and detection were conducted with the following profile: 2 min at 50°C (uracil-DNA glycosylase [UDG] treatment), 10 min at 95°C (predenaturation), and 40 cycles of 15 sec at 95°C, 30 sec at 60°C, and 30 sec at 72°C. The melt curve was performed immediately after the amplification protocol consisting of 60 melt cycles, starting at 65°C with increments of 0.5°C/cycle. The primers were as follows: *vegfaa*, FWD (5′-CCT CACCTGTAAATGCTCCTGC-3′) and REV (5′-CATCTT GGCTTTTCACATCTGC-3′); *vegfr2*, FWD (5′-CTGCTTTG ACTATTGATGAGAGGC-3′) and REV (5′-TGTGATAAA GGGTGCTGGAACTC-3′). The expression level was normalized to that of β-actin, amplified with the primer sequences: FWD (5′-GTCCGTGACATCAAGGAGAAGC-3′) and REV (5′-GAAACGCTCATTGCCGATGG-3′). Four embryos were used per treatment and all assays were performed in triplicates.

Statistical analysis

All IC_{50} values were analyzed by SPSS version 17. The mean and standard deviation (± 1 SD) was calculated and compared by one way analysis of variance or ANOVA with Tukey HSD. Statistical significance was defined when $p < 0.05$.

Results

Among the six crude cerumen extracts, a difference in mass, yield, and appearance were noticed with respect to the different solvents (Table 1). Overall, CDE had the highest yield (52.0%), while CME had the lowest yield (4.86%). It seemed that the order of solvent extraction did not affect the appearance of the crude extracts, where CDE and reCDE, CHE and rCHE, and CME and reCME, looked alike. However, the yield of each crude extract was affected by the order of sequential extraction. Furthermore, the six crude extracts affected the inhibition of each cancer cell line differently (Table 1). The SW620 cell line was the most sensitive to all the crude extracts (IC_{50} range of 0.55–0.57 μg/mL), while reCDE had the strongest cytotoxity against the five cancer-derived cell lines (IC_{50} range of 0.56–5.24 μg/mL).

Since reCDE was the most active crude extract, it was further fractionated by silica gel CC and, after pooling of those fractions that had the same TLC profile, yielded 16 fractions (F1–16). In addition to their different TLC profiles (data not shown), these 16 fractions had a different appearance and IC_{50} value for cytotoxicity against the five human cancer cell lines (Supplement 1). However, the IC_{50} value of each fraction (F1–16) was higher (lower activity) than that of the starting reCDE for each cell line, suggesting either the loss of more active compound(s) or the separation of synergistic compounds. Nevertheless, from the MTT assay, fractions F7 and F8 had the strongest cytotoxicity against the five human cancer-derived cell lines (IC_{50} range from 3.38 ± 2.18 to 6.46 ± 0.17 μg/mL and from 5.37 ± 0.57 to 6.60 ± 0.30 μg/mL, respectively) and so they were separately purified by silica gel CC. Fraction F7 (330 mg), which had been eluted with 60:40 (v/v) hexane: ethyl acetate, yielded, after pooling of fractions with the same TLC profile, 10 subfractions (F7A–J). In the same manner,

Table 1 Cytotoxic activity of the six crude cerumen extracts against five human cancer-derived cell lines

Crude extract	Mass (g)	Yield (%)	Appearance	IC_{50} value (μg/mL)*				
				BT474	Chago	Hep-G_2	KATO-III	SW620
CME	9.715	4.86	Brown liquid	6.95 ± 0.46^{a}	2.20 ± 1.10^{a}	0.87 ± 0.08^{a}	2.11 ± 0.97^{ab}	0.57 ± 0.02^{a}
CDE	103.994	52.0	Sticky, red-brown, resinous rubber	5.04 ± 0.22^{a}	0.95 ± 0.04^{a}	0.74 ± 0.05^{a}	3.63 ± 1.95^{ab}	0.55 ± 0.00^{a}
CHE	47.010	23.5	Sticky, yellow-brown wax	37.6 ± 3.6^{b}	6.97 ± 0.69^{b}	2.92 ± 1.48^{a}	2.42 ± 1.08^{ab}	0.57 ± 0.01^{a}
reCME	5.850	9.28	Brown liquid	56.6 ± 9.2^{c}	2.38 ± 1.51^{a}	0.84 ± 0.08^{a}	0.89 ± 0.05^{a}	0.57 ± 0.00^{a}
reCDE	19.020	30.1	Sticky, red-brown, resinous rubber	5.24 ± 0.27^{a}	1.53 ± 0.56^{a}	0.75 ± 0.04^{a}	0.78 ± 0.05^{a}	0.56 ± 0.01^{a}
reCHE	27.410	43.4	Sticky, yellow-brown wax	36.4 ± 4.9^{b}	4.89 ± 2.39^{ab}	0.92 ± 0.03^{ab}	5.21 ± 1.69^{b}	0.56 ± 0.00^{a}

*Data are shown as the mean ± 1SD, derived from three independent repeats. Means in the same column with a different lowercase letter have significantly different IC_{50} values ($p \leq 0.05$).
CME: crude methanol extract; CDE: crude dichloromethane extract; CHE: crude hexane extract; IC_{50}: 50% inhibition concentration; SD: standard deviation.

Table 2 Appearance and cytotoxicity IC_{50} values against five cancer cell lines of the active subfractions from the third silica gel CC fractionation of reCDE

Fraction	Mass (mg)	Yield (%)	Appearance	IC_{50} (μg/mL)*				
				BT474	Chago	Hep-G_2	KATO-III	SW620
F7E-3	31.4	15.3	Yellow crystal	0.50 ± 0.01^{a}	0.92 ± 0.08^{a}	0.39 ± 0.04^{a}	0.36 ± 0.06^{a}	0.62 ± 0.16^{a}
F7E-4	13.1	6.39	Yellow, oily	4.55 ± 0.21^{b}	8.13 ± 0.63^{b}	3.16 ± 0.81^{b}	7.24 ± 0.62^{c}	8.47 ± 0.83^{c}
F7E-5	39.8	19.4	Yellow, oily	3.31 ± 0.77^{b}	6.67 ± 1.58^{b}	6.36 ± 0.38^{c}	6.48 ± 0.78^{c}	6.48 ± 1.00^{c}
F7E-6	34.2	16.7	Yellow, oily	4.06 ± 0.62^{b}	8.46 ± 0.76^{b}	4.60 ± 0.14^{b}	4.41 ± 0.19^{b}	3.07 ± 0.14^{b}
F8E-5	10.2	5.10	Yellow, oily	1.94 ± 0.15^{a}	3.88 ± 0.10	1.93 ± 0.04	1.73 ± 0.26^{a}	1.68 ± 0.06^{a}
F8E-6	5.6	2.80	Red-brown solid	2.32 ± 0.49^{ab}	5.86 ± 0.89	5.37 ± 1.14	5.93 ± 1.54^{b}	7.07 ± 0.34^{a}
F8E-7	33.5	16.8	Red-brown solid	3.77 ± 0.73^{b}	> 10	> 10	7.07 ± 0.34^{b}	2.17 ± 0.05^{a}

*Data are shown as the mean ± 1SD, derived from three independent repeats. Means within a column with a different lowercase letter have significantly different IC_{50} values ($p \leq 0.05$).CC: column chromatography; IC_{50}: 50% inhibition concentration; SD: standard deviation.

F8 (300 mg) yielded nine (F8A–I) subfractions after silica gel CC. Among these 19 subfractions F7D, F7E, and F8E showed a high cytotoxicity against all five cancer cell lines, with IC_{50} values ranging from 0.88 ± 0.03 to 1.01 ± 0.03 μg/mL, 5.37 ± 0.57 to 6.60 ± 0.30 μg/mL, and 3.96 ± 1.93 to 6.28 ± 1.18 μg/mL, respectively (Supplement 2). In contrast, all the other subfractions had no marked cytotoxicity at all (data not shown).

Since the ^{1}H NMR spectra of subfractions F7D (22 mg) and F7E (216 mg), which had been eluted with 96.5:3.5 (v/v) DCM: MeOH, were similar but a greater yield of F7E was obtained, then subfraction F7E was further fractionated using silica gel CC (2.5 cm × 50 cm) and was eluted with DCM-MeOH in a stepwise fashion to give, after pooling of the fractions with the same TLC profile, 13 fractions (F7E-1 to F7E-13). Likewise, another 13 fractions (F8E-1 to F8E-13) were obtained from the subfraction of sample F8E. Thus, a total of 26 fractions were obtained. After screening them for cytotoxicity using the MTT assay, fractions F7E-3 to F7E-6 and fractions F8E-5 to F8E-7 were found to be active (Table 2). Fraction F7E-3 showed the strongest cytotoxicity against the five cancer cell lines, with IC_{50} values ranging between 0.36 ± 0.06 and 0.92 ± 0.08 μg/mL. Analysis of these fractions by ^{1}H and ^{13}C NMR revealed that fraction F7E-3 was a pure compound (α-mangostin), while fractions F7E-4, F7E-5, F7E-6, F8E-5, F8E-6, and F8E-7 contained α-mangostin as the main component together with small amount of impurity. Therefore, the main cytotoxic compound isolated from *T. laeviceps* cerumen was identifed by analysis of the spectroscopic data (1D- and 2D-NMR and HRESIMS) and comparison of their spectroscopic data with those reported in the literature[17] to be α-mangostin (Figure 1):

^{1}H NMR (400 MHz, $CDCl_3$): δ 1.69 (3H, s, CH_3-15), 1.77 (3H, s, CH_3-19), 1.83 (3H, s, CH_3-14), 1.84 (3H, s, CH_3-20), 3.46 (2H, br s, H-16), 3.80 (3H, s, 7-OMe), 4.10 (2H, br s, H-11), 5.26 (1H, m, H-12), 5.29 (1H, m, H-17), 6.30 (1H, s, H-4), 6.83 (1H, s, H-5) and 13.79 (1H, s, 1-OH) ^{13}C NMR (100 MHz, $CDCl_3$): δ 18.1 (C-20), 18.4 (C-14), 21.6 (C-16), 25.9 (C-19), 26.0 (C-15), 26.7 (C-11), 62.2 (7-OMe), 93.4 (C-4), 101.7 (C-5), 103.8 (C-9 a), 108.6 (C-2), 112.4 (C-8 a), 121.6 (C-17), 123.4 (C-12), 132.3 (C-13), 135.8 (C-18), 137.2 (C-8), 142.8 (C-7), 154.7 (C-10 a), 155.2 (C-4 a), 155.9 (C-6), 160.8 (C-1), 161.8 (C-3) and 182.2 (C-9). HRESIMS *m/z* 433.1646 [M+Na]+ (433.1627 calculated for $C_{24}H_{26}NaO_6$).

In order to determine the potential suitability of α-mangostin as an alternative chemotherapeutic drug, its cytotoxicity and effect upon cell proliferation, apoptosis, and migration in the five human cancer-derived cell lines was evaluated. We first compared its cytotoxicity

(as IC_{50} values) to those of 5-FU and doxil, two currently used chemotherapeutic drugs. Overall, doxil was numerically more effective (lower IC_{50} values) than α-mangostin in all the selected cell lines except for KATO-III (0.88 ± 0.16 μmol/L for α-mangostin and 1.03 ± 0.16 μmol/L for doxil), although doxil was not significantly better than α-mangostin on the BT474 and Hep-G_2 cell lines (Table 3). In contrast, 5-FU was only cytotoxic against the SW620 and Chago cell lines.

The morphology of α-mangostin treated cells (at its respective IC_{50} concentration) was observed at various incubation periods in terms of the nucleus and organelle condensation, cell shrinking, and cell floating. In brief, a similar pattern of morphological changes were observed in all the cell lines after treatment with α-mangostin. Just after the addition of α-mangostin (nominal 0 h), the treated cells started to shrink and change from a spindle to a round shape with condensation of the nucleus and organelle. At 24 h to 48 h of treatment, the number (density) of cells had decreased markedly, especially in the Chago cell line where the rapid decrease in cell density was easily noticed, while the number of dead cells increased. Meanwhile, cell debris started to appear within 48 h for BT474 and Hep-G_2 or within 24 h for Chago and SW620. After 72 h of incubation, the level of cell debris dramatically increased for the BT474, Hep-G_2, and SW620 cell lines. However, for KATO-III, at 72 h incubation, their morphology looked similar to that at 48 h and no debris was seen. In contrast, the morphology of the DMSO-only treated (control) cells remained as healthy spindle-shaped cells even after 72 h incubation. In addition, the density of the control cells increased over treatment time and was much more than the treated cells, especially for the Chago and SW620 cell lines where the control cells almost reached confluency. As an example, the morphology of the control and α-mangostin-treated SW620 cells are shown in Supplement 3.

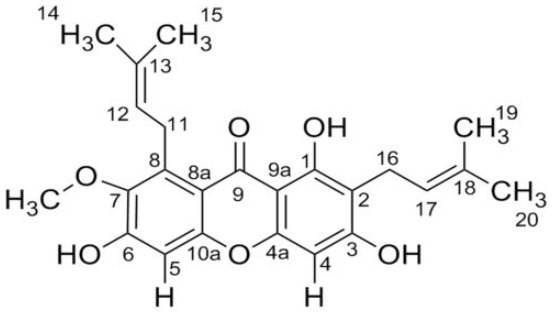

Figure 1 The deduced chemical structure of fraction F7E-3, as α-mangostin

Next, we sought to determine the effects of α-mangostin on the proliferation rates of normal (primary) and cancer-derived cell lines in real time using the RTCA platform. The HeLa, HT29, and primary fibroblast cells were seeded into E-plates 2–3 days prior to incubation with or without various concentrations of α-mangostin. The cells were then monitored every 30 min for the indicated period of time. Using the impedance-based real-time assay, we confirmed the dose-dependent growth inhibition of α-mangostin. As shown in Figure 2, treating cells with 20 μM α-mangostin led to a 72% and 57% decrease in growth rates of HeLa and HT29 cells, respectively, while only marginally affecting the proliferation of primary fibroblast cells (22%). Therefore, the cytotoxicity of α-mangostin may have some specificity to cancerous cells, but this awaits confirmation *in vitro* on other cell types as well as *in vivo*.

Since α-mangostin is known to strongly induce apoptosis in cancer cells,[13] we ascertained if α-mangostin induced cell death by caspase-dependent apoptosis by measuring the combined activity level of caspase-3 and -7. Treatment of HeLa or primary fibroblast cells with increasing concentrations of α-mangostin for 2 days did not result in any detectable activation of caspase-3/7 activity (Figure 3). Similar results were observed in the HT29 cells (data not shown). As a reagent control, SiHa cells treated with 7 and 14 μg/ml cisplatin for 48 h led to a 2.7- and 14.4-fold activation of caspase-3/7 activities, respectively (data not shown). Therefore, our data suggest that α-mangostin induces cell death in the cytotoxic susceptible cells via a caspase-independent mechanism.

We next asked whether α-mangostin could inhibit cell migration at low (nontoxic) concentrations. The migratory activity of the HeLa cell line in response to α-mangostin was assessed by the RTCA platform. As expected, untreated HeLa cells migrated from the upper chamber in FBS-free CM_D to the lower chamber containing CM_D (Figure 4). No significant change in the migration rates was observed when the cells were treated with 2.5 or 5 μM α-mangostin and so low (non-cytotoxic) concentrations of α-mangostin do not significantly alter cell motility.

Table 3 Comparison of IC_{50} values among doxil, 5-FU and α-mangostin

	IC_{50} (μg/mL)[§]			IC_{50} (μmol/L)*		
Drug Cell line	**Doxil**	**5-FU**	**α-Mangostin**	**Doxil**	**5-FU**	**α-mangostin**
BT474	0.42 ± 0.12	>10	0.50 ± 0.01	0.77 ± 0.21	>76.5	1.22 ± 0.03
Chago	0.35 ± 0.07	0.38 ± 0.08	0.92 ± 0.08	0.65 ± 0.14	2.91 ± 0.64	2.25 ± 0.20
Hep-G_2	0.32 ± 0.08	>10	0.39 ± 0.04	0.59 ± 0.15	>76.5	0.94 ± 0.01
KATO-III	0.56 ± 0.09	>10	0.36 ± 0.06	1.03 ± 0.16	>76.5	0.88 ± 0.16
SW620	0.07 ± 0.00	5.69 ± 0.79	0.62 ± 0.16	0.12 ± 0.00	43.5 ± 5.6	1.50 ± 0.39

*Data are shown as the mean ± 1SD, derived from three independent repeats. Means within a column with a different lowercase letter have significantly different IC_{50} values ($p \leq 0.05$). The MWs of doxil, 5-FU and α-mangostin are 543.5, 130.0 and 747.3 g mol^{-1}, respectively.
IC_{50}: 50% inhibition concentration; SD: standard deviation; 5-FU 5-fluorouracil.

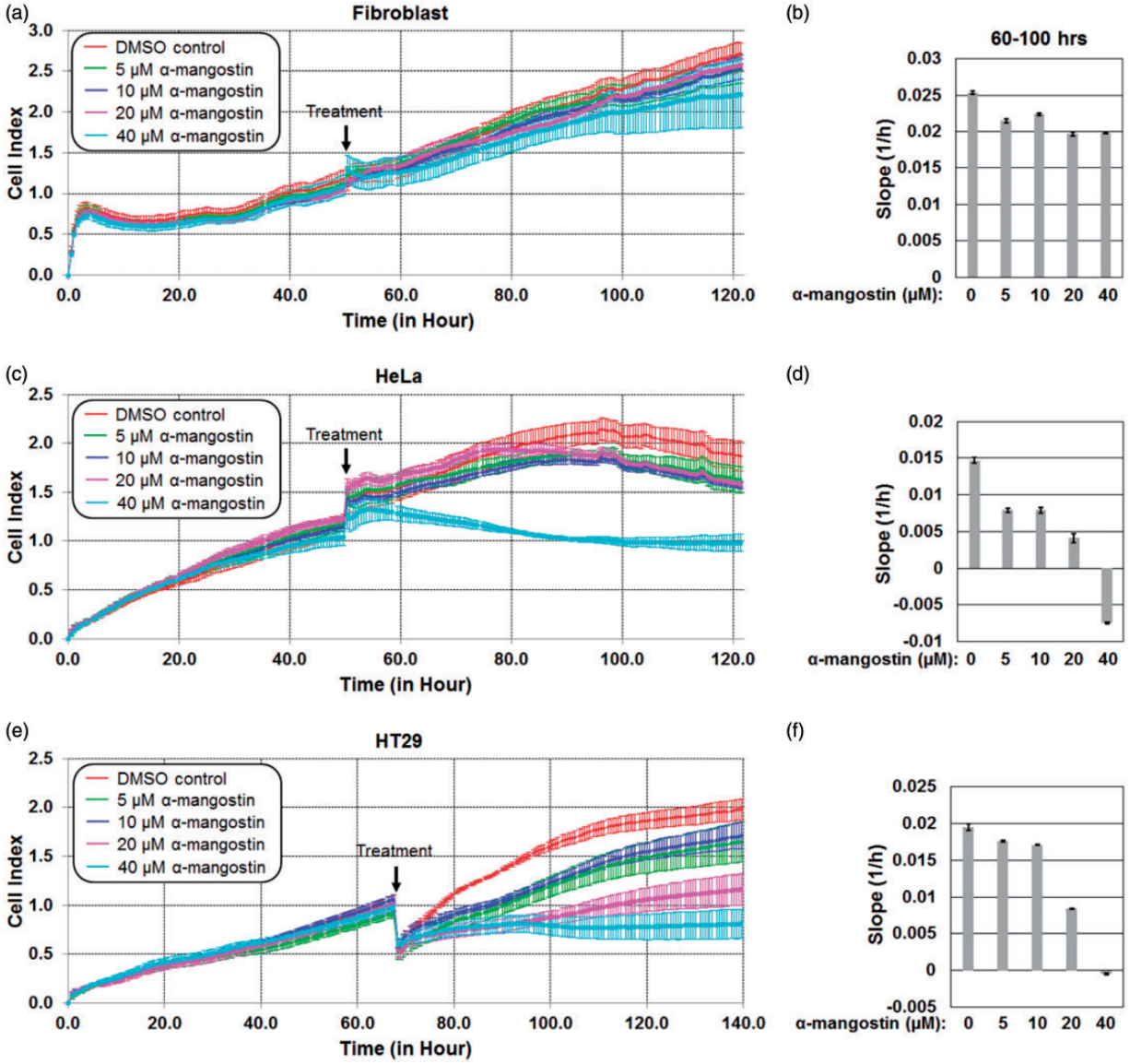

Figure 2 Dynamic real-time monitoring of the *in vitro* cytotoxicity of α-mangostin in normal and cancer-derived cell lines. Primary fibroblast, HeLa and HT29 cells were seeded in 96×E-plates at a density of 1500, 3000 and 5000 cells/well, respectively. The cells were continuously monitored until the cell index was approximately 1, at which point DMSO (control) or α-mangostin was then added (indicated by black arrows). The rate of proliferation was monitored in real time for 3 days post-treatment using the xCELLligence system. (a, c, and e) The rate of proliferation of (a, b) fibroblast, (c, d) HeLa, and (e, f) HT29 cells when incubated with DMSO or various concentrations (5, 10, 20 or 40 μM) of α-mangostin, shown as (a, c, and e) representative real-time cell index values and (b, d, and f) after analyzing the slope of the line between the indicated time intervals and shown as the mean ± 1 SD from triplicate replications. DMSO: dimethylsufoxide. (A color version of this figure is available in the online journal.)

To explore the anti-angiogenic properties of α-mangostin, we examined whether α-mangostin affected blood vessel development *in vivo* in zebrafish embryos. The survival of zebrafish embryos exposed to various concentrations of α-mangostin for 72 h was evaluated, and from this the LC_{50} value was derived and found to be 9.4 μM with a correlation coefficient (R^2) of 0.99 (Figure 5(a)). Then, the effect of continuous exposure of zebrafish embryos to 9 and 12 μM α-mangostin upon the formation of a neovascularized network in the SIV plexus was examined using the endogenous alkaline phosphatase activity of zebrafish endothelial cells. Alkaline phosphatase staining showed a normal SIV pattern in the control and α-mangostin-treated embryos (Figure 5(b)), although a quantitative analysis revealed a numerically slightly, but not statistically significant, decrease in the number of intersections in SIV (Figure 5(c)). Additionally, the relative transcript expression levels of the *vegfaa* and *vegfr2* genes in the α-mangostin-treated embryos, as determined by qrtRT-PCR were significantly decreased in the presence of 12 and 9 μM α-mangostin, respectively (Figure 5(d)). Thus, α-mangostin does not appear to exert an anti-angiogenic property in the zebrafish embryo model even though it negatively regulates the transcript expression level of *vegfaa* and *vegfr2*.

Discussion

Many bee products, especially honey, bee pollen, propolis, and cerumen, vary in their appearance and chemical composition depending upon the plant source. For propolis in Thailand, most is typically brown to dark brown in colour and contains cardanol and cardol as the main cytotoxic compounds.[14] In Brazil, green propolis and red propolis were reported, and they contained artepillin C and 3-hydroxy-8,9-dimethoxypterocarpan as the main bioactive compounds.[15,16] In contrast, red propolis in China was reported to contain chrysin, tectochrysin, pinocembrin, and galangin as the main bioactive compounds.[18] Here, cerumen from *T. laevicepes* in Thailand, which also had propolis as one of its components, looked yellow and brown, resembling the resin from mangosteen fruits and stem bark, and was found to contain α-mangostin with a potential strong anticancer activity. We speculate that cerumen, either in a raw or crude form, could be exploited in cancer chemoprevention and/or chemotherapy.

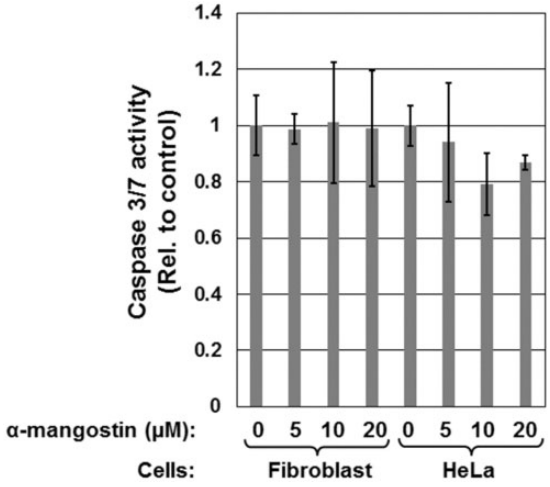

Figure 3 Effects of α-mangostin on caspase 3/7 activation. Primary fibroblast and HeLa cells grown in a 96-well plate were incubated with 0 (DMSO solvent control), 5, 10, or 20 μM α-mangostin and the combined caspase 3/7 activity level was quantified using the Caspase 3/7-Glo kit at 48 h post-treatment. Data were normalized to the caspase 3/7 activity of the solvent control and are shown as the mean $\pm$ 1 SD from quadruplicate replications

Although many reports have supported that the method of extraction plays an important role in obtaining bioactive compounds,[19,20] the sequence of solvents used here in the sequential extraction or cerumen did not affect the appearance of the obtained crude extract at all but did affect the obtained yield. Of the three different solvents, DCM seemed to be efficient for the extraction of bioactive compounds (in this study, cytotoxicity), which concurs with previous reports that the obtained CDE gave the best bioactivity.[21] Nonetheless, the enrichment of active compound(s) from bee products is considered to be simpler than that from plants.[22]

Here, the cytotoxic fraction F7F-3 from *T. laeviceps* cerumen was found to be α-mangostin ($C_{24}H_{26}O_6$), which belongs in the xanthone group.[23] This compound is known to have medical and pharmaceutical bioactivities, such as antioxidant,[24] antimicrobial,[25] anti-inflammatory,[26] and anticancer activities.[27] Although this compound was previously reported from the roots[17] and pericarp[28] of mangosteen, including those collected in Chantaburi province (Thailand), this is the first report of α-mangostin in Thai cerumen.

In addition to the conventional end-point cytotoxicity assay, we utilized RTCA for real-time analyses of the effect of α-mangostin on the proliferation rate of

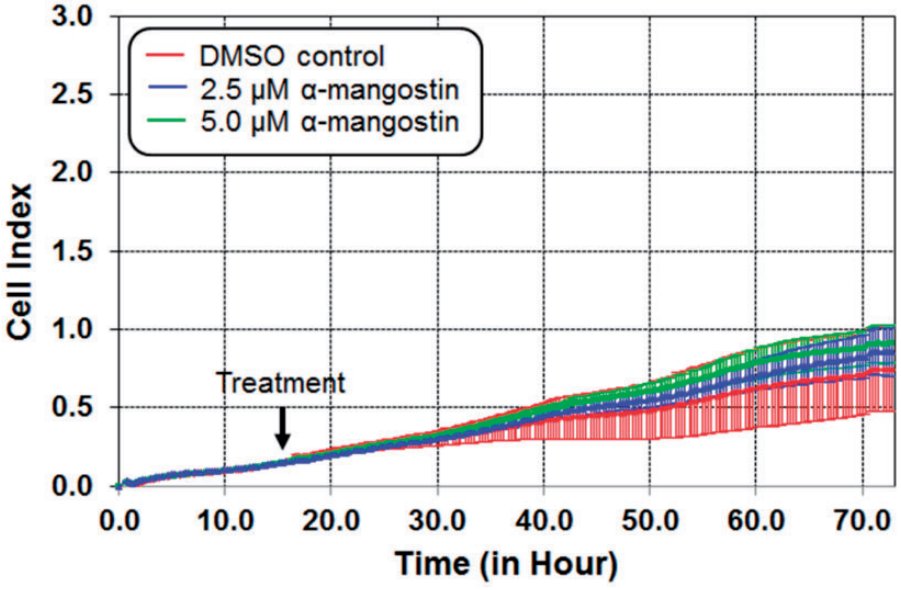

Figure 4 Real-time HeLa cell migration in response to α-mangostin. HeLa cells were seeded in FBS-CM_D for 16 h in the upper chamber of the CIM-plate. Subsequently, cells were treated with 0 (DMSO solvent control), 2.5 or 5 μM α-mangostin (see the Methods section). The rate of migration was monitored in real time using the xCELLigence system for a total of 72 h. Bars are the mean $\pm$ 1 SD, derived from triplicate assays. DMSO: dimethylsufoxide. (A color version of this figure is available in the online journal.)

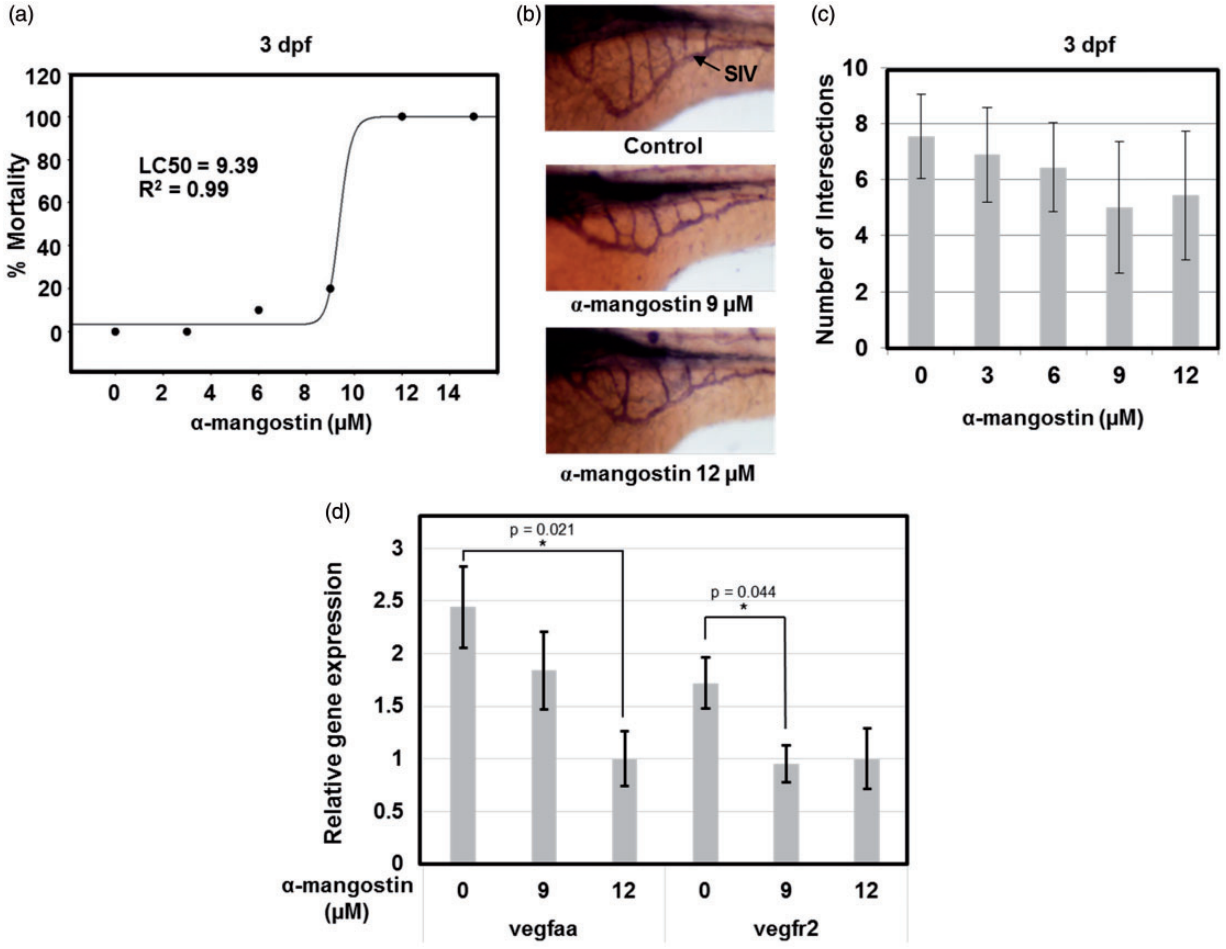

Figure 5 Effects of α-mangostin on zebrafish blood vessel development. (a) Representative LC_{50} of α-mangostin after the exposure to zebrafish embryos for 3 days. (b) Representative alkaline phosphatase stained embryos displaying subintestinal vessels (SIV) by 3 dpf. (c) The number of SIV plexus intersection points (mean $\pm$ 1 SD, derived from 10 embryos). (d) Transcript expression level of the *vegfaa* and *vgfr2* genes in the control and α-mangostin-treated embryos (mean$\pm$ 1 SD, derived from four embryos; $^*p < 0.05$; Student's *t*-test). (A color version of this figure is available in the online journal.)

cancer-derived cell lines versus a primary fibroblast cell line. An α-mangostin-mediated dose- and time-dependent growth inhibition was observed in both the HeLa and HT29 cell lines (Figure 2(c) and (e)), but the primary fibroblast cells were much less sensitive to the cytotoxic effects of α-mangostin than the cancer-derived cells, in agreement with a previous report in normal and lung cancer cell lines.[29] It has previously been shown that α-mangostin suppresses the expression and intracellular activity of fatty acid synthase, a metabolic enzyme commonly over-expressed in various cancer cell lines and crucial for their survival.[30] Additionally, α-mangostin can inhibit mammalian DNA polymerase and topoisomerases, which may also contribute to its stronger toxicity towards rapidly dividing cancer cells.[31] Our data support a potential chemopreventive and chemotherapeutic potential of α-mangostin for cancer treatment, but this requires further tissue specific and *in vivo* confirmation.

Despite suppressing cell proliferation, α-mangostin was reported to exert its antitumor activity through an activation of apoptosis.[13,31] Paradoxically, we did not observe any activation of the executioner caspase (caspase−3/7) activities in HeLa and HT29 cell lines incubated with up to 20 μM α-mangostin (Figure 3 and data not shown). A caspase-independent cell killing method has been documented previously in human colon cancer DLD-1 cells, where α-mangostin-induced apoptosis was mediated through the release of endonuclease-G from mitochondria.[13]

The potential anti-metastasis property of α-mangostin was preliminarily evaluated via cell migration assays using the RTCA system. Using the CIM-plates, the kinetics of HeLa cell migration in the absence and presence of low (nontoxic) concentrations of α-mangostin was monitored. In contrast to a previous report in pancreatic cancer cells,[32] we did not observe any significant effect of α-mangostin on the migration rate of HeLa cells (Figure 4). This discrepancy could be attributed to differences in cell lines or concentrations of α-mangostin used. It is plausible that α-mangostin might possess anti-migratory activity in some types of (cancer) cell lines when used at higher concentrations.

Finally, we elucidated the effects of α-mangostin on the *in vivo* angiogenesis of zebrafish embryos as a vertebrate model. Zebrafish have been used as a model for

toxicological studies,[33] drug screening,[34] and human diseases.[35] Zebrafish possesses a complex circulatory system that is morphologically and physiologically similar to that of mammals.[36] Moreover, they have a highly characteristic blood vessel pattern in the developing embryo and the SIV can be stained and visualized microscopically. The toxicity of α-mangostin in zebrafish embryos was found to have an LC_{50} at 72 h of 9.4 μM (Figure 5(a)), which is the first report of the LC_{50} of α-mangostin in zebrafish embryos, and so the *in vivo* inhibition of angiogenesis was evaluated in this concentration range (9 and 12 μM). In addition, since *Vegfaa* is a major regulator in angiogenesis that binds to and activates two tyrosine kinase receptors (*vegfr1* and *vegfr2*) that regulate pathological and physiological angiogenesis, the effect of α-mangostin upon their transcript expression level was monitored. Although α-mangostin was found to decrease the transcript expression levelss of *vegfaa* and *vegfr2* (Figure 5(d)), it did not affect the angiogenic phenotypes of zebrafish embryos (Figure 5(b) and (c)). It is possible that the slight decrease in *vegfaa* and *vegfr2* transcript levels induced by αmangostin was not sufficient to inhibit *in vivo* angiogenesis. Alternatively, functional redundancy of other components involved in the angiogenic pathway, such as *vegfr1*, may have alleviated the anti-angiogenic effects of α-mangostin.

In summary, the cerumen of *T. laeviceps* from Chantaburi province (Thailand) contains α-mangostin, which possesses a potent *in vitro* anticancer activity across a broad range of human cancer-derived cell lines. Its cytotoxicity was much more pronounced against cancerous than normal cells and is likely to be mediated by suppressing cell proliferation and inducing caspase-independent apoptosis. We suggest that Thai stingless bee cerumen may have chemopreventive benefits and prove useful as an adjuvant therapy or as an alternative medicine for the treatment of multiple malignancies.

Author contributions: PN conducted the cerumen purification and cell cytotoxicity assays. SP helped in cell culture. TI designed and conducted the real-time cytotoxicity and cell migration assays, caspase assay, gene expression analysis, and wrote the manuscript. WP designed and conducted the zebrafish assays and wrote the manuscript. SP designed the provided overall advice in chemistry and wrote the manuscript. CC supplied the cerumen and α-mangostin material, helped design the experiments, provided overall advice in biology, and wrote the manuscript. All authors read and approved the final manuscript.

ACKNOWLEDGEMENTS

We thank Dr. Robert Butcher for assisting in manuscript preparation. This work was supported by the 90th Anniversary of Chulalongkorn University Fund (Ratchadaphiseksomphot Endowment Fund), the Ratchadapisek Sompoch Endowment Fund of Chulalongkorn University (RES560530041-FW and CU-56-019-FC), and internal funding from the National Nanotechnology Center (NANOTEC).

DECLARATION OF CONFLICTING INTERESTS

The author(s) declared no potential conflicts of interest with respect to the research, authorship, and/or publication of this article.

REFERENCES

1. Sakagami S, Inoue T. Taxonomic notes on three bicolorous *Tetragonula* stingless bees in Southeast Asia. *Jpn J Entomol* 1985;**53**:174–89
2. Klakasikorn A, Wongsiri S, Deowanish S, Duangphakdee O. New record of stingless bees (Meliponini: *Trigona*) in Thailand. *NHJCU* 2005;**5**:1–7
3. Roubik DW. Stingless bee nesting biology. *Apidologie* 2006;**37**:124–43
4. Simone-Finstrom M, Spivak M. Propolis and bee health: the natural history and significance of resin use by honey bees. *Apidologie* 2010;**41**:295–11
5. Jo M, Park MH, Kollipara PS, An BJ, Song HS, Han SB, Kim JH, Song MJ, Hong JT. Anti-cancer effect of bee venom toxin and melittin in ovarian cancer cells through induction of death receptors and inhibition of JAK2/STAT3 pathway. *Toxicol Appl Pharmacol* 2012;**258**:72–81
6. Alves de Souza S, Camara CA, Monica Sarmento da Silva E, Silva TM. Composition and antioxidant activity of geopropolis collected by *Melipona subnitida* (Jandaíra) bees. *Evid Based Complement Alternat Med* 2013;**2013**:801383
7. Massaro FC, Brooks PR, Wallace HM, Russell FD. Cerumen of Australian stingless bees (*Tetragonula carbonaria*): gas chromatography-mass spectrometry fingerprints and potential anti-inflammatory properties. *Naturwissenschaften* 2011;**98**:329–37
8. Uzel A, Sorkun KY, Oncag O, Cogulu D, Gencay O, Salih B. Chemical compositions and antimicrobial activities of four different Anatolian propolis samples. *Microbiol Res* 2005;**160**:189–95
9. Kanwar JR, Mahidhara G, Kanwar RK. Antiangiogenic therapy using nanotechnological-based delivery system. *Drug Discov Today* 2011;**16**:188–02.
10. Zhong S, Li W, Chen Z, Xu J, Zhao J. MiR-222 and miR-29a contribute to the drug-resistance of breast cancer cells. *Gene* 2013;**531**:8–14
11. Newman DJ, Cragg GM. Natural products as sources of new drugs over the last 25 years. *J Nat Prod* 2007;**70**:461–77
12. Zoeller JJ, McQuillan A, Whitelock J, Ho SY, Iozzo RV. A central function for perlecan in skeletal muscle and cardiovascular development. *J Cell Biol* 2008;**181**:381–94
13. Nakagawa Y, Iinuma M, Naoe T, Nozawa Y, Akao Y. Characterized mechanism of alpha-mangostin-induced cell death: caspase-independent apoptosis with release of endonuclease-G from mitochondria and increased miR-143 expression in human colorectal cancer DLD-1 cells. *Bioorg Med Chem* 2007;**15**:5620–8
14. Teerasripreecha D, Phuwapraisirisan P, Puthong S, Kimura K, Okuyama M, Mori H, Kimura A, Chanchao C. In vitro antiproliferative/cytotoxic activity on cancer cell lines of a cardanol and a cardol enriched from Thai *Apis mellifera* propolis. *BMC Complement Altern Med* 2012;**12**:27
15. Hata T, Tazawa S, Ohta S, Rhyu MR, Misaka T, Ichihara K, Artepillin C. A major ingredient of Brazilian propolis, induces a pungent taste by activating TRPA1 channels. *PLoS One* 2012;**7**:1–7
16. Daugsch A, Moraes CS, Fort P, Park YK. Brazilian red propolis – chemical composition and botanical origin. *Evid Based Complement Alternat Med* 2008;**5**:435–41
17. Ghazali MSIAS, Lian CEG, Ghani ADK. Chemical constituent from roots of *Garcinia mangostana* (Linn.). *Int J Chem* 2010;**2**:134–42
18. Hatano A, Nonaka T, Yoshino M, Ahn MR, Tazawa S, Araki Y, Kumazawa S. Antioxidant activity and phenolic constituents of red propolis from Shandong, China. *Food Sci Technol Res* 2012;**18**:577–84
19. Bankova V, Trusheva B, Trunkova D. Different extraction methods of biologically active components from propolis: a preliminary study. *Chem Cent J* 2007;**1**:13
20. Khacha-ananda S, Tragoolpua K, Chantawannakul P, Tragulpua Y. Antioxidant and anti-cancer cell proliferation activity of propolis

extracts from two extraction methods. *Asian Pac J Cancer Prev* 2013;**14**:6991–5
21. Marchetti MG, Silva AK, Santos NA, Sousa OMI, Tinti VS, Figueira MG, Foglio AM, Carvalho EJ. The anticancer activity of dichloromethane crude extract obtained from *Calea pinnafida*. *J Exp Pharmacol* 2012;**4**:157–62
22. Abdennacer B, Karim M, Yassine M, Nesrine R, Mouna D, Mohamed B. Determination of phytochemicals and antioxidant activity of methanol extracts obtained from the fruit and leaves of Tunisian Lycium intricatum Boiss. *Food Chem* 2015;**174**:577–84
23. Soda M, Endo S, Matsunaga T, Zhao HT, El-Kabbani O, Iinuma M, Yamamura K, Hara A. Inhibition of human aldose reductase-like protein (AKR1B10) by alpha- and gamma-mangostins, major components of pericarps of mangosteen. *Biol Pharm Bull* 2012;**35**:2075–80.
24. Chin YW, Jung HA, Chai H, Keller WJ, Kinghorn AD. Xanthones with quinone reductase-inducing activity from the fruits of *Garcinia mangostana* (Mangosteen). *Phytochemistry* 2008;**69**:754–58
25. Sundaram BM, Gopalakrishnan C, Subramanian S, Shankaranarayanan D, Kameswaran L. Antimicrobial activities of *Garcinia mangostana*. *Planta Med* 1983;**48**:59–60
26. Chen LG, Yang LL, Wang CC. Anti-inflammatory activity of mangostin from Garcinia mangostana. *Food Chem Toxicol* 2008;**46**:688–93
27. Matsumoto K, Akao Y, Ohguchi K, Ito T, Tanaka T, Iinuma M, Nozawa Y. Xanthones induce cell-cycle arrest and apoptosis in human colon cancer DLD-1 cells. *Bioorg Med Chem* 2005;**13**:6064–9
28. Watanapokasin R, Jarinthanan F, Nakamura Y, Sawasjirakij N, Jaratrungtawee A, Suksamran S. Effects of alpha-mangostin on apoptosis induction of human colon cancer. *World J Gastroenterol* 2011;**17**:2086–5
29. Shih YW, Chien ST, Chen PS, Lee JH, Wu SH, Yin LT. Alpha-mangostin suppresses phorbol 12-myristate 13-acetate-induced MMP-2/MMP-9 expressions via alphavbeta3 integrin/FAK/ERK and NF-kappaB signaling pathway in human lung adenocarcinoma A549 cells. *Cell Biochem Biophys* 2010;**58**:31–4
30. Li P, Tian W, Ma X. Alpha-mangostin inhibits intracellular fatty acid synthase and induces apoptosis in breast cancer cells. *Mol Cancer* 2014;**13**:138
31. Mizushina Y, Kuriyama I, Nakahara T, Kawashima Y, Yoshida H. Inhibitory effects of alpha-mangostin on mammalian DNA polymerase, topoisomerase and human cancer cell proliferation. *Food Chem Toxicol* 2013;**59**:793–80
32. Xu Q, Ma J, Lei J, Duan W, Sheng L, Chen X, Hu A, Wang Z, Wu Z, Wu E, Ma Q, Li X. Alpha-mangostin suppresses the viability and epithelial-mesenchymal transition of pancreatic cancer cells by downregulating the PI3K/Akt pathway. *Biomed Res Int* 2014;**2014**:article ID 546353
33. Dai YJ, Jia YF, Chen N, Bian WP, Li QK, Ma YB, Chen YL, Pei DS. 2014. Zebrafish as a model system to study toxicology. *Environ Toxicol Chem* 2014;**33**:11–7
34. Rennekamp AJ, Peterson RT. 15 years of zebrafish chemical screening. *Curr Opin Chem Biol* 2015;**24**:58–70
35. Blackburn JS, Langenau DM. Zebrafish as a model to assess cancer heterogeneity, progression and relapse. *Dis Model Mech* 2014;**7**:755–62.
36. Hu N, Sedmera D, Yost HJ, Clark EB. Structure and function of the developing zebrafish heart. *Anat Rec* 2000;**260**:148–57

(Received June 3, 2015, Accepted July 16, 2015)